SAND2019-14690C

High-Magnification, Long-Working Distance Plenoptic Background Oriented Schlieren (BOS)

Daniel R. Guildenbecher[1], William M. Kunzler[2], William C. Sweatt[3], and Katya M. Casper[4]
Sandia National Laboratories, Albuquerque, New Mexico, 87125, USA

The design, construction, and testing of a high-magnification, long working-distance plenoptic camera is reported. A plenoptic camera uses a microlens array to enable resolution of the spatial and angular information of the incoming light field. Instantaneous images can be numerically refocused and perspective shifted in post-processing to enable three-dimensional (3D) resolution of a scene. Prior to this work, most applications of plenoptic imaging were limited to relatively low magnifications (1× or less) or small working distances. Here, a unique system is developed with enables 5× magnification at a working distance of over a quarter meter. Experimental results demonstrate ~25 μm spatial resolution with 3D imaging capabilities. This technology is demonstrated for 3D imaging of the shock structure in a underexpanded, Mach 3.3 free air jet.

I. Introduction

A plenoptic camera uses a microlens array to discretize the spatial and angular distribution of the light rays that pass through an objective lens. In post-processing, images can be digitally refocused to different optical depths and perspective shifted. Following the development of a practical and compact plenoptic camera by Ng *et al.*[1], this technology has been applied for several diagnostic science applications including three-dimensional (3D) profilometry[2], velocimetry[3,4], particle tracking[5-8], in-cylinder measurements[9], pyrometery[10], etc. Most of these applications utilize commercially available plenoptic systems or a combination of commercially available objective lenses and/or microlens arrays. Consequently, image magnifications are typically either rather low (1× or less) or, in the case of high-magnification systems, are limited to relatively small working distances (on the order of mm) defined by typical microscope objectives. For applications involving harsh environments, such as the fires and supersonic flows considered here, critical microscopic features cannot be resolved at the long working-distances required to protect equipment.

This work reports on the design and application of a customized plenoptic system that enables 5× magnification at a working distance of 260 mm. This is applied to perform a 3D Background Oriented Schlieren (BOS) measurement of the shock structure in Mach 3.3 free air jet. BOS images a stationary background. Index of refraction gradients that exist between the background and the camera cause an apparent shift in the background pattern. By tracking this shift, the index-of-refraction field is visualized[11]. BOS has been traditionally performed with standard (non-plenoptic) camera systems. Consequently, BOS typically only provides a 2D line of sight visualization of the refraction field. Recently, the combination of BOS and plenoptic cameras has extended this to a 3D measurement[12]. Such plenoptic-BOS measurements have certain advantages compared to alternative 3D BOS techniques that utilize multiple tomographic cameras[13].

[1] Research Engineer, Diagnostic Science & Engineering, AIAA Senior Member.
[2] Research Engineer, Diagnostic Science & Engineering
[3] Research Engineer, Fluid and Reactive Processes
[4] Research Engineer, Aerosciences, AIAA Senior Member.

II. Experiment Design and Configuration

The effort to design and build a high-magnification, long-working distance plenoptic system began with the optical performance requirements listed in Table 1. These requirements were selected to enable imaging of features with spatial scales on the order of ~100 μm at working distances compatible with the cross-sectional size of wind-tunnel facilities at Sandia National Laboratories[14,15].

Table 1. Desired performance of a high-magnification, long-working distance plenoptic system.

in-plane resolution, $\Delta x \leq 30$ μm
depth resolution, $\Delta z \leq 200$ μm
total depth range, DOF ≥ 5 mm
working distance, $l_o = 260$ mm

The governing equations for the performance of a plenoptic imaging system have been derived elsewhere[1]. Here, the design considerations most relevant to the current configuration are briefly reviewed. The current design is based on a plenoptic 1.0 configuration in which a micro-lens array (MLA) is placed one micro-lens focal length away from the image sensor. As described by Ng *et al.*[1], the MLA results in the recording of sub-images that locally discretize the angular distribution of light through the main lens aperture. As first described by Ng *et al.*[1] these results can be post-processed to either numerically refocus or shift the perspective of an instantaneous image.

To ensure that the micro-lenses record the full solid angle of the main lens aperture, the image side *f*-number of the main lens should match the *f*-number of the micro-lenses[16]

$$\frac{l_i}{d} = \frac{f_\mu}{p_\mu}. \tag{1}$$

The right hand side of Eq. (1) is the *f*-number of the micro-lenses where f_μ is the focal length of the micro-lenses and p_μ is the pitch (diameter) of the micro-lenses. The left-hand side defines the image side *f*-number of the main lens where f is the focal length and l_i is the image distance. These quantities are related to the object distance, l_o, via the lens equation

$$\frac{1}{f} = \frac{1}{l_o} + \frac{1}{l_i}, \tag{2}$$

with optical magnification given by

$$m = \frac{-l_i}{l_o}. \tag{3}$$

As derived by Deem *et al.* [17], the depth of field (depth resolution) of a numerically refocused image (determined by the shifted summation of all information under each micro-lens) is given by

$$\Delta z = \frac{f\left(m-1\right)^2}{m\left(m-1\right) - f_\mu n / f\left(n-2\right)} - \frac{f\left(m-1\right)^2}{m\left(m-1\right) + f_\mu / f}, \tag{4}$$

where n is the number of image sensor pixels behind each micro-lens,

$$n = \frac{p_\mu}{p_p}, \tag{5}$$

and p_p is the pixel pitch. The in-plane resolution is discretized by the micro-lenses such that the effective in-plane resolution is the magnified size of the micro-lenses in object space

$$\Delta x = p_\mu / |m| \tag{6}$$

A perspective shifted image is calculated by selecting one pixel behind each micro-lens. The effective aperture of the perspective shifted image, d_{eff}, is therefore n times smaller than the main lens aperture

$$d_{eff} = \frac{d}{n} = \frac{l_i p_p}{f_\mu} \tag{7}$$

As discussed by Ng *et al.* [1], the depth of field (DOF) of a perspective image can be determined from traditional DOF equations using this effective aperture. Here, a simplified version valid at large magnification is used

$$DOF = \frac{2 f p_\mu \left(1-m\right)}{d_{eff} m^2} \tag{8}$$

Equations (1)-(8) define a system of eight equations with thirteen variables (f, m, d, l_o, l_i, p_p, p_μ, f_μ, n, d_{eff}, Δx, Δz, DOF) which govern the design and performance of a plenoptic camera. By fixing any five variables, Eq. (1)-(8) can be solved for the remaining eight.

To begin, consider the plenoptic camera that we have used in our previous works[5-8]. This camera was designed for image magnifications around m = -1. A f = 105 mm Nikon front objective is used in conjunction with a custom MLA (p_μ = 77 μm, f_μ = 308 μm) along with a CCD with p_p = 5.5 μm. At the desired imaging distance (l_o = 260 mm), Eqs. (1)-(8) indicate that this system is capable of achieving a magnification of m = -0.67, depth resolution of Δz = 1.5 mm, and in-plane resolution of Δx = 0.11 mm, all of which are significantly worse than the desired performance parameters in Table 1. If instead, the existing MLA and CCD is retained (p_μ = 77 μm, f_μ = 308 μm, p_p = 5.5 μm) and Eqs. (1)-(8) is optimized to achieve the desired imaging distance (l_o = 260 mm) and in-plane resolution (Δx = 30 μm), the resulting system would require a custom front objective and would achieve a depth resolution of Δz = 101 μm but only enable a total usable DOF of 1.3 mm.

Meeting all desired performance characteristics, therefore requires a new MLA along with a custom front objective. Here, we assume that only the existing CCD is retained (p_p = 5.5 μm) and Eqs. (1)-(8) are solved to meet the desired performance characteristics (l_o = 260 mm, Δx = 30 μm, Δz = 200 μm, DOF = 5 mm). The resulting system includes a custom MLA with p_μ = 143 μm and f_μ = 2.19 mm. Furthermore, a custom front objective is required with relatively high-magnification, m = -4.8, and large aperture, d = 81 mm.

Due to cost and time constraints, it was decided to purchase a commercial off-the-shelf (COTS) MLA and focus development efforts on the design of the front objective. After searching various COTS suppliers, the best available COTS MLA was determined to be P/N MLA-S125-f15 from RCP Photonics with a micro-lens pitch of p_μ = 125 μm and focal length of f_μ = 1.875 mm.

A custom objective lens was designed and optimized in Zemax®. The design consists of a four-element lens group, which was manufactured by Quality Thin Films in Tampa, Florida. The predicted performance of the as-designed system is summarized in Table 2. Notice that the total depth range (DOF) in Table 2 is somewhat smaller than the desired range in Table 1 due to the use of the COTS MLA. In the future, a custom MLA could be purchased to ultimately meet all desired performance characteristics.

Table 2. Predicted performance of the as-built system.

front objective	**Micro-lens array (MLA)** (RCP P/N MLA-S125-f15)	**predicted performance**
focal length, f = 215.4 mm working distance, l_o = 260 mm magnification, m = -4.80 aperture, d = 84 mm	focal length, f_μ = 1.875 mm pitch, p_μ = 125 μm	in-plane resolution, Δx = 26 μm depth resolution, Δz = 170 μm total depth range, DOF = 3.7 mm

The customized plenoptic system is shown in Fig. 1. In this development effort, the four lenses forming the front objective are free-space mounted using typical opto-mechanical hardware. Translation stages with micrometers are used to adjust the inter-lens separations to match the Zemax® design. In addition, the MLA is mounted immediately in front of the CCD camera with alignment controlled by a custom tip-tilt mount provided by Auburn University.

Fig. 1. The custom, high-magnification, long-working-distance plenoptic system.

The optical performance of the front objective (without MLA) is first characterized by imaging a metrology grade dot grid with known dimensions. The measured image magnification is between -4.7 to -4.9 where the variations are due to system realignment during development. In addition, up to group 5 element 2 of a 1951 USAF optical resolution chart could be fully resolved. This indicates a spatial resolution of 35 lp/mm or 14 μm. As is discussed in the next section, the resolution of the front objective is better than the predicted in-plane resolution, Δx, of the complete plenoptic system (with MLA). This indicates that the micro-lens pitch, p_μ, is the ultimate limiter of system optical resolution.

Having confirmed that the front objective performs as predicted in the first column in Table 2, the remainder of this work discuss the performance characterization and application of the complete high-magnification, long-working distance plenoptic system (with MLA).

III. Results and Analysis

To demonstrate the system operation, Fig. 2 shows a raw plenoptic image of an ant mounted on a pinhead. Fig. 2(a) shows the full image, while Fig. 2(b) shows a zoomed-in region highlighting the sub-aperture images recorded by the MLA.

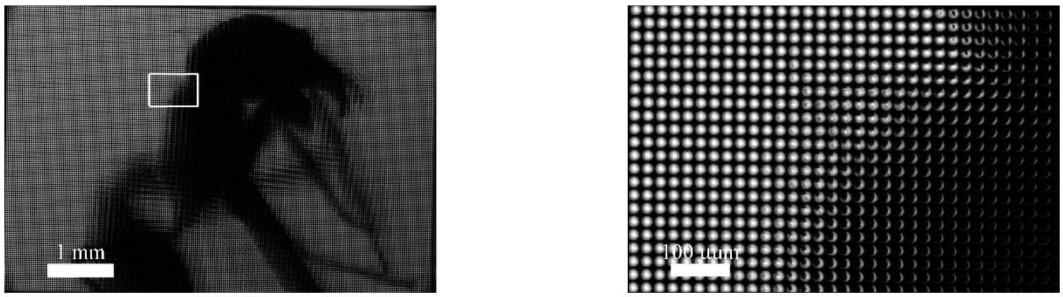

(a) (b)

Fig. 2. (a) Raw plenoptic image of an ant mounted on a pinhead and (b) a zoomed-in region showing the sub-images created by the MLA.

Fig. 3 shows perspective shifted (left) and numerically refocused (right) results found by post-processing the single raw plenoptic image shown in Fig. 2. Processing methods are described extensively elsewhere[1,5-8]. In the perspective shifted images on the left, notice how the location of the mandibles in the foreground shifts with respect to the legs in the background. In the refocused images on the right, the optical depth, z, with respect to the nominal focal plane is shown in the upper left. In this work, the main lens focal length and magnification are used along with the thin lens equation (Eq. (2)) to determine these optical depths[5]. Notice how the legs in the background are in better focus at an optical depth further away from the nominal focal plane (positive z, bottom) while the mandibles are in better focus closer to the camera (negative z, top).

Although qualitative, the images in Fig. 3 are consistent with the predicted optical performance in the third column in Table 2. The depth resolution, Δz, estimates the accuracy with which objects can be located in the optical depth direction from refocused images. On the right of Fig. 3, small objects, particularly the hair located on the back, are well-focused within a sub-mm depth region as predicted in Table 2. In addition, the DOF quantifies the total optical depth wherein objects are in-focus in the perspective shifted images. In this example, the object likely spans a total optical depth of a few mm. Most of the features on the left-hand side of Fig. 3 appear to be in-focus within this few mm range, again qualitatively confirming the predicted DOF given in Table 2. Finally, the in-plane resolution, Δx, is confirmed by imaging a 1951 USAF optical resolution chart with the complete plentoptic system. Up to group 4 element 2 is resolved. This corresponds to a spatial resolution of 18 lp/mm or about 28 μm. This closely matches the predicted Δx in Table 2 confirming that the magnified size of the MLA pitch, p_μ, is the ultimate limiter of the in-plane spatial resolution (via Eq (6)).

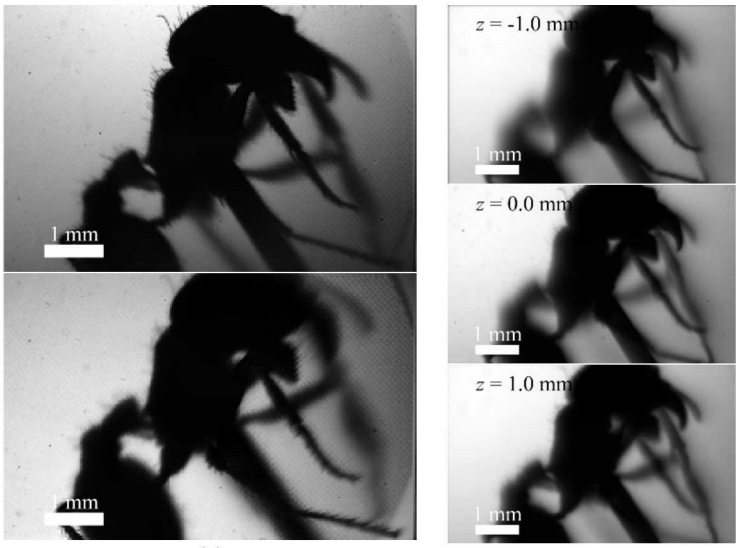

(a) (b)

Fig. 3. (a) perspective shifted and (b) numerically refocused images from the raw image in Fig. 2.

As discussed in the previous section, a distinguishing feature of the system presented here is the long-working distance (260 mm or ~10.2"). This presents advantages for difficult measurement environments where large standoff is required to protect optics and/or image into test facilities.

To demonstrate imaging in harsh conditions, consider the environment created by the combustion of an aluminized solid-rocket fuel. It is well known that aluminum particulate tends to melt and agglomerate at the burning surface. This particulate is subsequently ejected into the product gases where agglomerates combust at high-temperature (on the order of 3000 K)[18]. Knowledge of the size distribution of aluminum agglomerates is needed to predict rocket motor performance[19] as well as address safety concerns[20]. Previously we have applied digital inline holography (DIH) for 3D imaging and quantification of size distributions when the solid-rocket fuel burns at atmospheric pressure[21-23]. However, as operating pressure increases toward more relevant conditions for rocket motor applications, laser based DIH fails due to susceptibility to image degradation via index-of-refraction gradients. In a related application, we have previously shown that plenoptic imaging is much less susceptible to these issues due to the use of white light illumination[7,8]. However, prior to the current work, it was not possible to resolve the aluminum agglomerates, which are on the order of 100 μm in diameter, using available plenoptic cameras at a safe working distance.

To explore high-magnification plenoptic imaging of a burning propellant, a small stick (~6 mm diameter and 50 mm long) was placed within the field of view of the plenoptic camera developed here. The scene was back illuminated with a pulsed diode (640 nm center wavelength, ±10 nm bandwidth, 2.5 μs pulse duration) and images were captured as the propellant burned through the FOV. Fig. 4 shows results from a single, instantaneous recording. In the perspective shifted images on the left, notice how the large burning agglomerate in the background shifts relative to the burning surface in the foreground. With appropriate calibration, these perspective shifts can be used to quantify three-dimensional particle locations as established in Hall *et al.*[7]. Similarly, the right-hand images in Fig. 4 show numerically refocused results, which also demonstrate an ability to resolve object locations based on focus[8]. Overall, the result in Fig. 4 are the first-known application of plenoptic imaging to this environment. Such a measurement would not be possible with previous plenoptic imaging configurations, which have either insufficient magnification[1,3-10,12,17] or insufficient standoff[16].

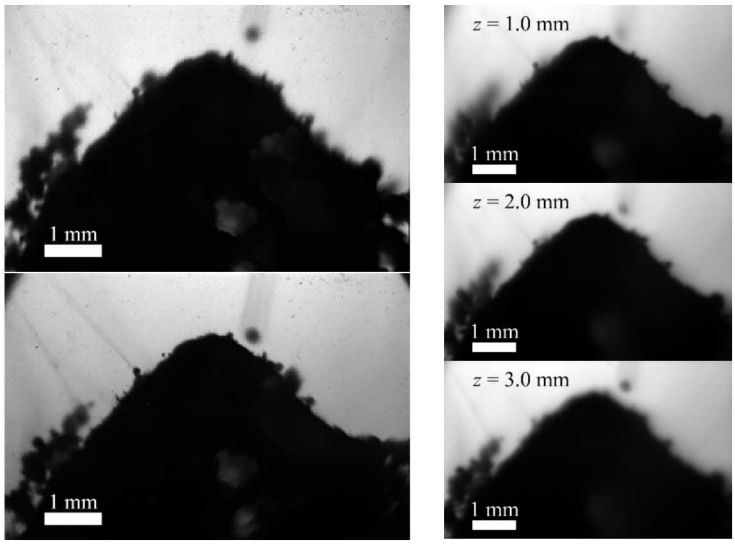

(a) (b)

Fig. 4. (a) perspective shifted and (b) numerically refocused images of the burning surface of an aluminized solid-rocket propellant.

Finally, the high-magnification, long-working distance plenoptic configuration is applied to demonstrate progress toward 3D resolution of index-of-refraction gradients. Fig. 5 shows results from a knife-edge schlieren configuration imaging a Mach 3.3 free air jet. The left-hand image of Fig. 5 was recorded with a vertical knife edge, resulting in the visualization of horizontal index-of-refraction gradients. Conversely, the right-hand image of Fig. 5 was recorded with a horizontal knife edge to visualize the index-of-refraction gradients along the vertical direction. Knife-edge schlieren images, such as Fig. 5, produce line-of-sight integrated results. Consequently, these images do not provide information on the optical depth location of the jet.

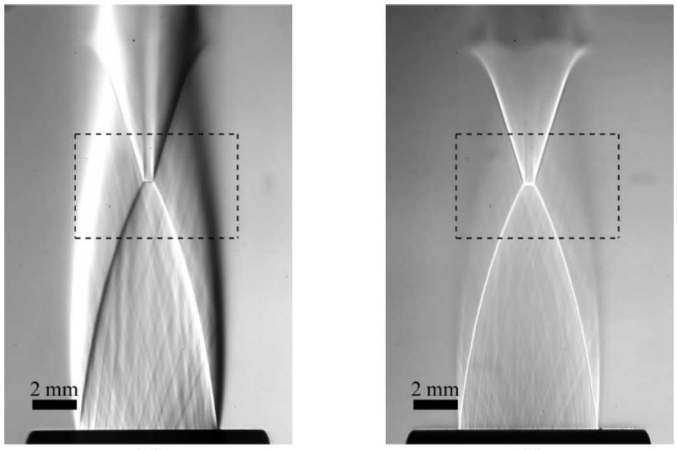

(a) (b)

Fig. 5. Knife-edge schlieren of a Mach 3.3 air jet. (a) vertical knife edge and (b) horizontal knife edge. Dotted lines show the approximate FOV of the plenoptic BOS configuration

Recently Klemkowsky *et al*[12] demonstrated plenoptic Background Oriented Schlieren (BOS) for 3D depth resolution from a single plenoptic camera. This technique quantifies the apparent motion of a stationary background placed behind the index-of-refraction gradients. In the current work, the DOF of the plenoptic configuration is relatively short. Consequently, a fixed background pattern cannot be placed directly at the focal plane without disturbing the air jet. Instead, a second, matching high-magnification lens system is used to relay the background to the nominal focal plane of the plenoptic configuration. The jet was then placed 10 mm closer to the camera with respect to focal plane.

Fig. 6 shows central perspective images of the background pattern utilized here. The left image of Fig. 6 shows the background with the jet off, while the right-hand size was recorded with the jet on. Careful study of these two images reveals small apparent motion between the left and right images.

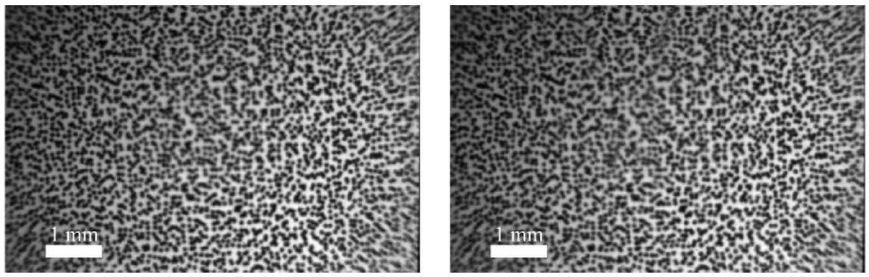

(a) (b)

Fig. 6. Central perspective image of plenoptic BOS showing (a) the reference image with jet off and (b) with jet on.

Using optical flow techniques inherited from commercial Digital Image Correlation (DIC) software, the apparent motion of the dot pattern shown in Fig. 6 is quantified as shown in Fig. 7. The left-hand image shows the measured displacement in the horizontal direction while the right-hand image shows the vertical displacements. These images can be compared with the corresponding FOV in the knife-edge schlieren results given by the dotted lines in Fig. 5. These results demonstrate that the high-magnification, long-working distance plenoptic BOS configuration visualizes the index-of-refraction gradients similarly to traditional knife edge schlieren. The signal-to-noise ratio in plenoptic BOS results (Fig. 7) is clearly lower than the corresponding knife edge schlieren (Fig. 5). The knife edge schlieren results are recorded with an effective pixel size of ~7.5 μm, while the plenoptic BOS configuration likely has a minimal spatial resolution on the order of ~50 μm (determined by the effective pixel size, Δx, and the spatial accuracy of the optical flow tracking). Results presented here are intended as a proof-of-principle of high-magnification, long-working distance plenoptic BOS. It is believed that signal-to-noise ratios could be improved with further system optimization.

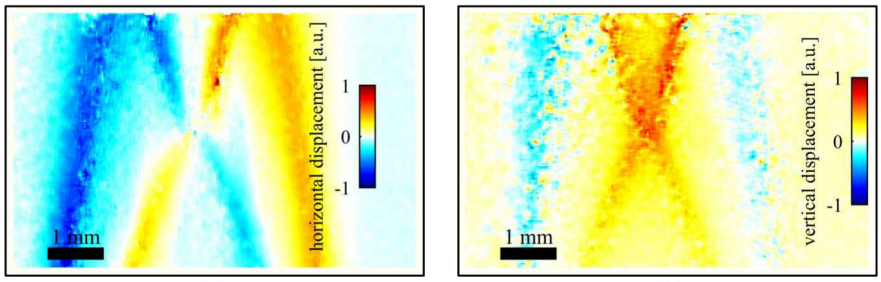

(a) (b)

Fig. 7. Measured apparent displacements in the (a) horizontal and (b) vertical directions of the central perspective image such as Fig. 6.

The main advantage of the plenoptic BOS configuration is to enable 3D resolution of density gradients from a single camera. This unique capability is demonstrated in Fig. 8 where the measured image displacements are numerically "refocused" using the methodology of Klemkowsky *et al*[12]. Again, the left-hand column shows the refocused horizontal displacements while the right-hand shows the vertical displacements. The air jet was located at z = -10 mm from the nominal focal plane, and indeed it is apparent that the measured displacements are maximum at this plane. Fig. 8 also shows that at ± 5 mm from the correct z, measured displacements are smeared. If desired, it seems that automated routines could be constructed to locate the index-of-refraction gradient to well within ± 5 mm.

Again, it should be noted that the results presented here are intended for proof-of-principle. The literature contains alternative 3D BOS reconstruction routines[11,13], which may be better suited to the 3D reconstruction of index-of-refraction. In addition, as already mentioned, system optimization may be possible through variation in the chosen background pattern (Fig. 6), disturbance location, correlation routines, etc. Such effort is left for future work.

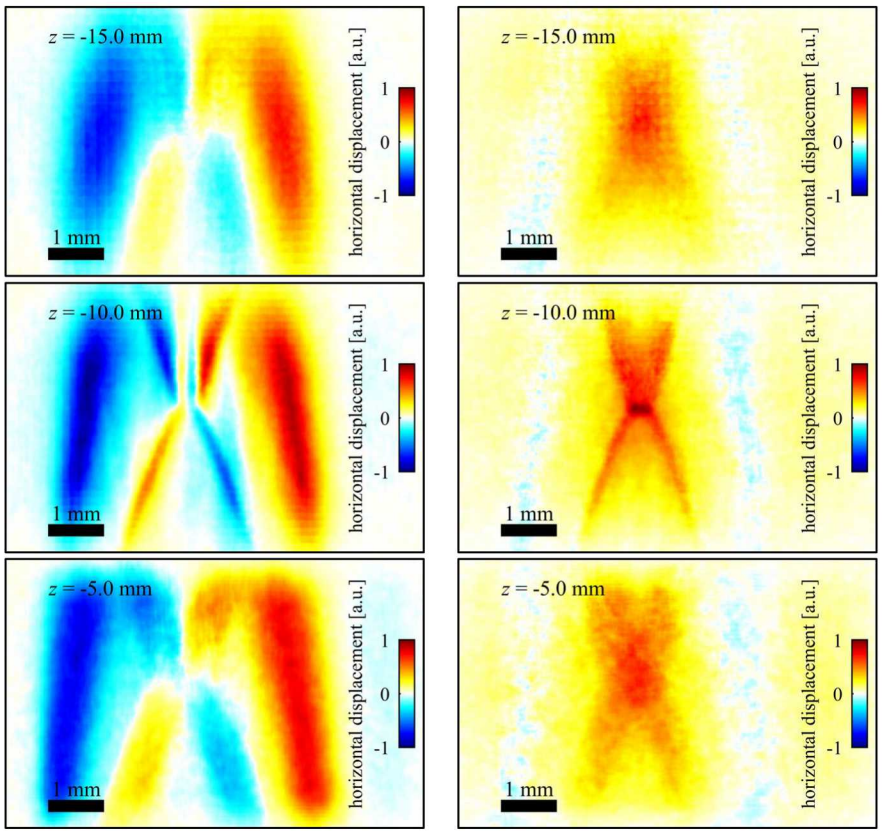

Fig. 8. Numerical "refocusing" of the plenoptic BOS displacements in the (a) horizontal and (b) vertical directions.

IV. Conclusion

A high-magnification, long-working-distance plenoptic configuration has been designed, constructed, and applied for 3D imaging of a lab-scale solid propellant fire and 3D Background Oriented Schlieren (BOS). Compared to previous high-magnification plenoptic configurations, the techniques presented here have the distinct advantage of a long-working distance (greater than 0.25 m) and high-magnification (5×). This enables single-camera, 3D diagnostics of harsh environments, where the standoff is needed to protect equipment, and flows within experimental facilities with medium to large cross-sections.

Acknowledgments

The authors gratefully acknowledge Professor Brian S. Thurow, Jenna N. Klemkowsky, and Elise M. Hall for their advice and assistance with experimental design and data processing. This work was supported by the Laboratory Directed Research and Development (LDRD) program at Sandia National Laboratories. This paper describes objective technical results and analysis. Any subjective views or opinions that might be expressed in the paper do not necessarily represent the views of the U.S. Department of Energy or the United States Government. Sandia National Laboratories is a multimission laboratory managed and operated by National Technology & Engineering Solutions of Sandia, LLC, a wholly owned subsidiary of Honeywell International Inc., for the U.S. Department of Energy's National Nuclear Security Administration under contract DE-NA0003525.

References

[1]Ng, R., Levoy, M., Bredif, M., Duval, G., Horowitz, M., and Hanrahan, P. "Light field photography with a hand-held plenoptic camera." Stanford University, 2005.

[2]Cai, Z., Liu, X., Tang, Q., Peng, X., and Gao, B. Z. "Light field 3D measurement using unfocused plenoptic cameras," *Optics Letters* Vol. 43, No. 15, 2018, pp. 3746-3749.

[3]Fahringer, T., and Thurow, B. "Tomographic reconstruction of a 3-D flow field using a plenoptic camera," *42nd AIAA Fluid Dynamics Conference and Exhibit*. American Institute of Aeronautics and Astronautics, 2012.
[4]Lynch, K., Fahringer, T. W., and Thurow, B. "Three-dimensional particle image velocimetry using a plenoptic camera," *50th AIAA Aerospace Sciences Meeting including the New Horizons Forum and Aerospace Exposition*. American Institute of Aeronautics and Astronautics, 2012.
[5]Hall, E. M., Fahringer, T. W., Guildenbecher, D. R., and Thurow, B. S. "Volumetric calibration of a plenoptic camera," *Applied Optics* Vol. 57, No. 4, 2018, pp. 914-923.
[6]Hall, E. M., Guildenbecher, D. R., and Thurow, B. S. "Uncertainty characterization of particle location using a plenoptic camera," *Optics Express* Vol. 25, No. 18, 2017, pp. 21801-21814.
[7]Hall, E. M., Guildenbecher, D. R., and Thurow, B. S. "Development and uncertainty characterization of 3D particle location from perspective shifted plenoptic images," *Optics Express* Vol. 27, No. 6, 2019, pp. 7997-8010.
[8]Hall, E. M., Thurow, B. S., and Guildenbecher, D. R. "Comparison of three-dimensional particle tracking and sizing using plenoptic imaging and digital in-line holography," *Applied Optics* Vol. 55, No. 23, 2016, pp. 6410-6420.
[9]Lillo Peter, M., Greene Mark, L., and Sick, V. "Plenoptic single-shot 3D imaging of in-cylinder fuel spray geometry," *Zeitschrift für Physikalische Chemie*. Vol. 229, 2015, p. 549.
[10]Fahringer, T. W., Danehy, P. M., and Hutchins, W. D. "Design of a multi-Color plenoptic camera for snapshot hyperspectral imaging," *2018 Aerodynamic Measurement Technology and Ground Testing Conference*.
[11]Raffel, M. "Background-oriented schlieren (BOS) techniques," *Experiments in Fluids* Vol. 56, No. 3, 2015, p. 60.
[12]Klemkowsky, J. N., Fahringer, T. W., Clifford, C. J., Bathel, B. F., and Thurow, B. S. "Plenoptic background oriented schlieren imaging," *Measurement Science and Technology* Vol. 28, No. 9, 2017, p. 095404.
[13]Atcheson, B., Ihrke, I., Heidrich, W., Tevs, A., Bradley, D., Magnor, M., and Seidel, H.-P. "Time-resolved 3D capture of non-stationary gas flows," *ACM Trans. Graph.* Vol. 27, No. 5, 2008, pp. 1-9.
[14]Casper, K. M., Beresh, S. J., Henfling, J. F., Spillers, R. W., Pruett, B. O. M., and Schneider, S. P. "Hypersonic wind-tunnel measurements of boundary-layer transition on a slender cone," *AIAA Journal* Vol. 54, No. 4, 2016, pp. 1250-1263.
[15]Steven, B., Sean, K., Justin, W., Daniel, G., John, H., Russell, S., Brian, P., Naibo, J., Mikhail, S., Jason, M., and Sukesh, R. "Pulse-burst PIV in a high-speed wind tunnel," *Measurement Science and Technology* Vol. 26, No. 9, 2015, p. 095305.
[16]Kim, J., Jeong, Y., Kim, H., Lee, C.-K., Lee, B., Hong, J., Kim, Y., Hong, Y., Lee, S.-D., and Lee, B. "F-number matching method in light field microscopy using an elastic micro lens array," *Optics Letters* Vol. 41, No. 12, 2016, pp. 2751-2754.
[17]Deem, E., A., Zhang, Y., Cattafesta, L., N., Fahringer, T. F., and Thurow, B. S. "On the resolution of plenoptic PIV," *Measurement Science and Technology* Vol. 27, No. 8, 2016, p. 084003.
[18]Price, E. W., and Sigman, R. K. "Combustion of aluminized solid propellants," *Solid propellant chemistry, combustion, and motor interior ballistics*. American Institute of Aeronautics and Astronautics, 2000, pp. 663-687.
[19]Jackson, T. L. "Modeling of heterogeneous propellant combustion: a survey," *AIAA Journal* Vol. 50, No. 5, 2012, pp. 993-1006.
[20]Height, J. L., Donaldson, B. A., Gill, W., and Parigger, C. G. "Measurements in solid propellant plumes at ambient conditions," *ASME 2011 International Mechanical Enigneering Congress & Exposition*. ASME, Denver, Colorado, USA, 2011.
[21]Guildenbecher, D. R., Cooper, M. A., Gill, W., Stauffacher, H. L., Oliver, M. S., and Grasser, T. W. "Quantitative, three-dimensional imaging of aluminum drop combustion in solid propellant plumes via digital in-line holography," *Optics Letters* Vol. 39, No. 17, 2014, pp. 5126-5129.
[22]Kearney, S. P., and Guildenbecher, D. R. "Temperature measurements in metalized propellant combustion using hybrid fs/ps coherent anti-Stokes Raman scattering," *Applied Optics* Vol. 55, No. 18, 2016, pp. 4958-4966.
[23]Chen, Y., Guildenbecher, D. R., Hoffmeister, K. N. G., Cooper, M. A., Stauffacher, H. L., Oliver, M. S., and Washburn, E. B. "Study of aluminum particle combustion in solid propellant plumes using digital in-line holography and imaging pyrometry," *Combustion and Flame* Vol. 182, 2017, pp. 225-237.